




Structural, optical, and electrochromic properties of RT and annealed sputtered tungsten trioxide (WO₃) thin films for electrochromic applications by using GLAD technique

K. Naveen Kumar^{1,2,*} , Sheik Abdul Sattar^{1,*}, G. V. Ashok Reddy^{1,*}, R. Imran Jafri³, R. Premkumar⁴, M. R. Meera⁵, A. Asrar Ahamed⁶, M. Muthukrishnan⁷, Merum Dhananjaya⁸, and Ammar M. Tighezza⁹

¹ Department of Physics, Nitte Meenakshi Institute of Technology, Yelahanka, Bengaluru 560064, India

² Centre for Nano-Materials and MEMS, Nitte Meenakshi Institute of Technology, Yelahanka, Bengaluru 560064, India

³ Department of Physics and Electronics, Christ University, Hosur Road, Bengaluru 560029, India

⁴ Department of Physics, N.M.S.S.V.N. College, Nagamalai, Madurai, Tamil Nadu 625019, India

⁵ Department of Physics, Sree Ayyappa College for Women, Chunkankadai, Nagercoil, Tamil Nadu 629 003, India

⁶ Department of Chemistry, Jamal Mohamed College (Autonomous), Affiliated to Bharathidasan University Trichy, Tiruchirappalli, Tamil Nadu 620020, India

⁷ Department of Physics, Sona College of Technology, Salem, Tamil Nadu 636005, India

⁸ School of Mechanical Engineering, Yeungnam University, 280 Daehak-ro, Gyeongsangbuk-do 38541, Republic of Korea

⁹ Department of Chemistry, College of Science, King Saud University, P. O. Box 2455, 11451 Riyadh, Saudi Arabia

Received: 23 June 2023

Accepted: 9 September 2023

Published online:
4 October 2023

© The Author(s), under exclusive licence to Springer Science+Business Media, LLC, part of Springer Nature, 2023

ABSTRACT

Tungsten oxide (WO₃) thin films were prepared on the GLAD DC magnetron sputtering (GDMS) and substrate angles were varied from 70° to 80°. The WO₃ thin films were deposited at room temperature (RT) on corning glass (CG) and fluorine-doped tin oxide (FTO), and substrates and annealed at 400 °C/2 h. The XRD, Uv–Vis spectrometer, and electrochemical analyzer were used to determine the structural, optical, and electrochromic (EC) properties. According to an XRD study, RT-deposited samples were amorphous, but annealed samples displayed crystalline structures. The optical transmittance of RT and annealed samples varied from 59 to 71% and 14 to 28% respectively. The colored/bleached ability of the cyclic voltammograms was RT samples shows greater than in annealed samples. Since the coloration ability and diffusion coefficient of WO₃ RT samples show greater than annealed samples.

Address correspondence to E-mail: naveenkilari95@gmail.com; sheik.abdul.sattar@nmit.ac.in; ashokreddy.gv@nmit.ac.in

<https://doi.org/10.1007/s10854-023-11285-x>

1 Introduction

WO₃ is a transition metal oxide material and it is an n-type semiconductor material bandgap of 2.6–3 eV and it is best for EC applications [1–3]. WO₃ has been drawn to its high coloration efficiency, high chemical stability, fast switching kinetics, and good electrochemical activity. It is possible to flip between the transparent and dark blue states optically when ions and electrons are simultaneously intercalation and deintercalation. The following Eq. (1) could be used to describe the EC mechanism of WO₃ films.



where WO₃ is EC layer, M⁺ are K⁺, Li⁺, Na⁺ and H⁺. *e*⁻ is the no of electrons. Other applications are solar cells [4], photodetectors [5], sensors for toxic gases [6], and ozone detectors [7]. Various deposition methods have successfully fabricated the Tungsten oxide (WO₃) thin film such as DC/RF magnetron sputtering [8–17], Electron beam evaporation [18, 19], Thermal evaporation [20], GLAD [21] and hydrothermal process [22–27]. Among the aforementioned methods, Glancing Angle Deposition (GLAD) is thought of as a flexible vapor-deposition method to regulate the various nanostructures by adjusting the substrate angle and revolution with relation to incoming vapour flux. The deposited films display various morphologies, displaying various physical and optical properties, depending on the revolution speed and substrate angle. GLAD Technique is the best for growing nanorods, nanostructures, zigzag columns, and nano springs [28]. The growth of WO₃ nanostructures from micro to nanoscales can be regulated using the GLAD deposition method. The density, shape, and size of nanocolumnar structured WO₃ films are controlled by the GLAD sputtering approach by modifying the process parameters [29–31]. The surface area for ion transport and electron intercalation/deintercalation is increased in nanostructured WO₃ films, which also have higher colouring efficiency, greater optical contrast ratio, and faster switching speed [32]. Yuan et al. have reported, the amorphous as-deposited films shown a high colouring efficiency and stable reversibility in comparison to annealed WO₃ porous nanostructured films.

They concluded that amorphous films exhibit greater colouring efficiency and larger optical modulation at 500 nm thickness [33]. Rydosz et al. were deposited the WO₃ thin films using GLAD method at various substrate angles with constant power. As can be observed, the optical parameters such as transmission and reflections change after annealing [34]. Steele, Brett has reported explaining the fabrication of advanced nanostructures with the GLAD technique [35]. The literature concludes that the nanostructured films show a stability, high diffusion coefficient, higher coloration efficiency and fast response than denser films.

In this paper, WO₃ films were deposited by using the GDMS at RT and substrate angles were varied from 70° to 80° and annealed at 400 °C/2 h. Optical, structural, and EC properties were determined by using a Uv–Vis spectrometer, XRD and an electrochemical analyzer.

2 Experimental details

WO₃ films were coated on CG and FTO substrates by using the GDMS. FTO and CG substrates were washed ultrasonically and dried with nitrogen gas. The sputtering chamber was evacuated 2×10^{-6} mbar by using the backing pump as a turbo molecular pump connected to a mechanical pump as a rotary pump. The reactive chamber's target was a 3-inch-diameter pure tungsten metal disc. In the chamber, the flow rates of pure oxygen as the reactive gas and argon as the working gas were maintained at 6 sccm and 25 sccm, respectively. The distance from the substrate to the metal target (9 cm), and the DC power were all held constant in this experiment. The only variable was the substrate angle, which varied from 70° to 80°. Both the base vacuum and the deposition vacuum were kept at 2×10^{-6} mbar and 1×10^{-2} mbar, respectively. The tungsten metal target was pre-sputtered in an argon environment for 10 min to get rid of the contaminants that had been adsorbed before sputtering. WO₃ films were deposited at RT and annealed at 400 °C/2 h at different substrate angles from 70° to 80°.

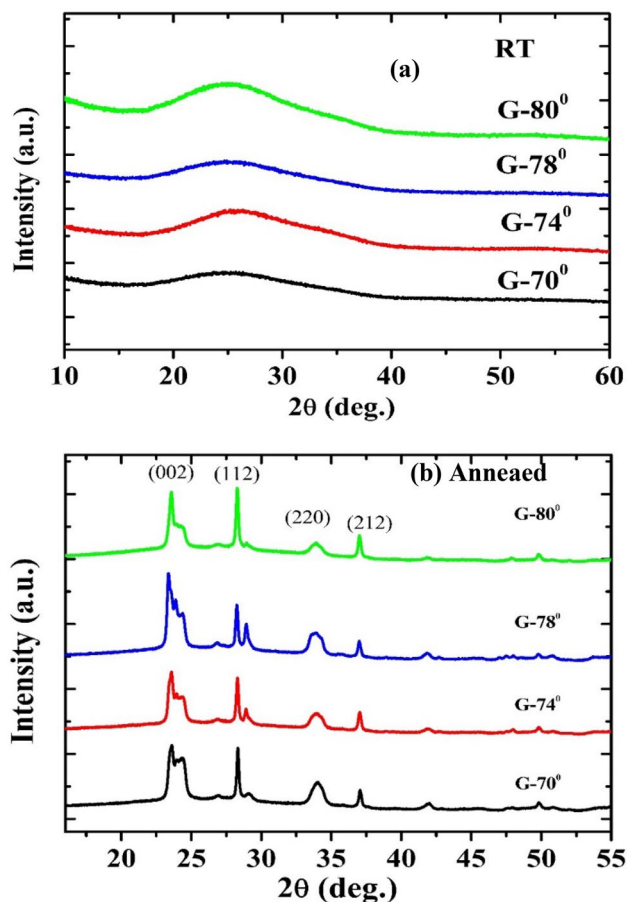


Fig. 1 XRD samples of a RT and b annealed WO₃ films

3 Results and discussion

3.1 Structural properties

The XRD plots of WO₃ films were deposited on CG substrates by using the GDMS at different substrates angles from 70° to 80° are shown in Fig. 1. Figure 1a shows the XRD pattern of the room temperature-deposited sample. Since no heating was applied during the preparation process, the tungsten ions combined with the oxygen ions at a lower energy level and reached the substrate surface. This resulted in the broad peaks that were seen in the XRD data, which confirms the film's amorphous nature. Figure 1b shows the annealed samples with a crystalline

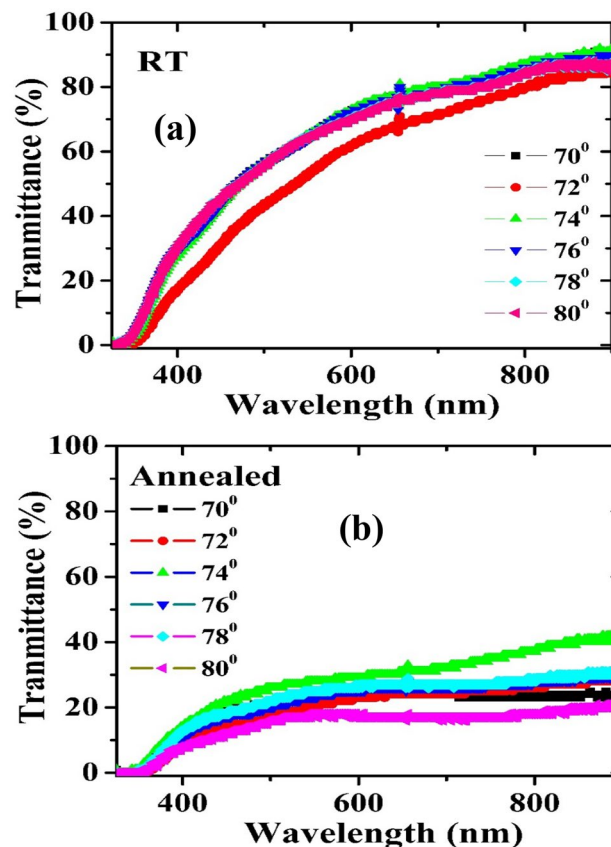


Fig. 2 Optical transmittance spectra of WO₃ films a RT and b annealed

structure and the majority of the peaks have a monoclinic crystal structure. The crystalline Peak intensities are (002), (112), (220), and (212) in the 2θ= 23.50°, 28.36°, 34.89°, and 37.78° [36] respectively.

3.2 Optical properties

The transmittance spectra of WO₃ films deposited on FTO and CG substrates by using the GDMS technique at different substrates angles from 70° to 80° are shown in Fig. 2. The transmittance spectra of RT samples show high transmittance of 58 to 72% (at λ = 600 nm) and annealed samples show less transmittance of 13 to 29% (at λ = 600 nm). The RT-deposited samples were showing more transmittance compared to annealed

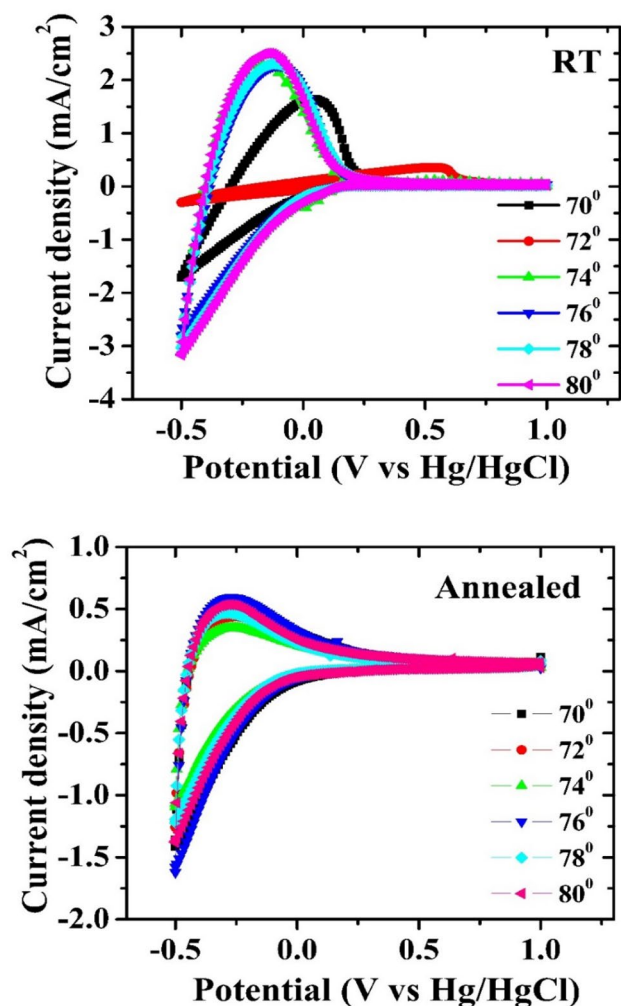


Fig. 3 Cyclic voltammograms of WO_3 films **a** RT and **b** annealed

samples. This is because RT samples have a more porous structure compared to the annealed samples.

3.3 Electrochromic properties

The EC properties of WO_3 films have been performed by using an electrochemical analyzer sp300 and which contains working, reference, and counter electrodes. Cyclic voltammograms (CV) of WO_3 films deposited at RT and annealed at $400\text{ }^\circ\text{C}/2\text{ h}$ samples are shown in Fig. 3. The WO_3 films as the working electrode, Pt

as a counter electrode, and Hg/HgCl is a reference electrode. The electrolyte solution of $0.5\text{ M H}_2\text{SO}_4$ was prepared. By applying voltages between -0.5 V to 1 V and Voltage scan rate was maintained at 10 mV/s for all RT and post-annealed samples CV curves show when negative potential (-0.5 V) was reached the H^+ ions were intercalated into the Active electrode area of WO_3 (EC layer) thin films. During this time color of the WO_3 thin film will change from transparent to blue color and optical transmittance was very less because more H^+ ions are accommodated in the WO_3 (EC layer) thin film. Again, when positive potential (1 V) was reached the H^+ ions were de-intercalated into the active electrode area of WO_3 (EC layer) thin films. During this time color of the WO_3 (EC layer), thin-film will change from blue color to transparent and optical transmittance was high, because fewer H^+ ions are accommodated in the WO_3 (EC layer) thin film. RT sample at GLAD angle 76° shows that more H^+ ions were intercalated and de-intercalated because the surface-to-volume ratio is more and porosity also more. An annealed sample at a GLAD angle 76° shows that more H^+ ions were intercalated and de-intercalated because the surface-to-volume ratio is more and porosity also more compared to other GLAD angles. RT samples show high oxidation and reduction peak currents compared to annealed samples. The reason was that RT samples show a highly porous structure compared to annealed samples. It can be expected from the above results that RT samples show high transmittance due to being more porous and annealed samples show less transmittance due to less porosity. Figures 4 and 5 shows the optical transmittance spectra of the as-deposited, colored and bleached state of WO_3 thin films deposited by various substrate angles from 70° to 80° . GLAD Angle 76° shows the transmittance of RT and bleached states are nearly the same due to high porosity. Optical transmittance spectra of annealed samples show the transmittance of RT and bleached states are nearly the same for all glad angles. Because after annealing the porosity will decrease for all glad angles and its forms a dense film with less porosity.

Figure 6 shows the coloration efficiency (CE) of WO_3 films on variation in wavelength and comparison between RT and annealed samples at various GLAD

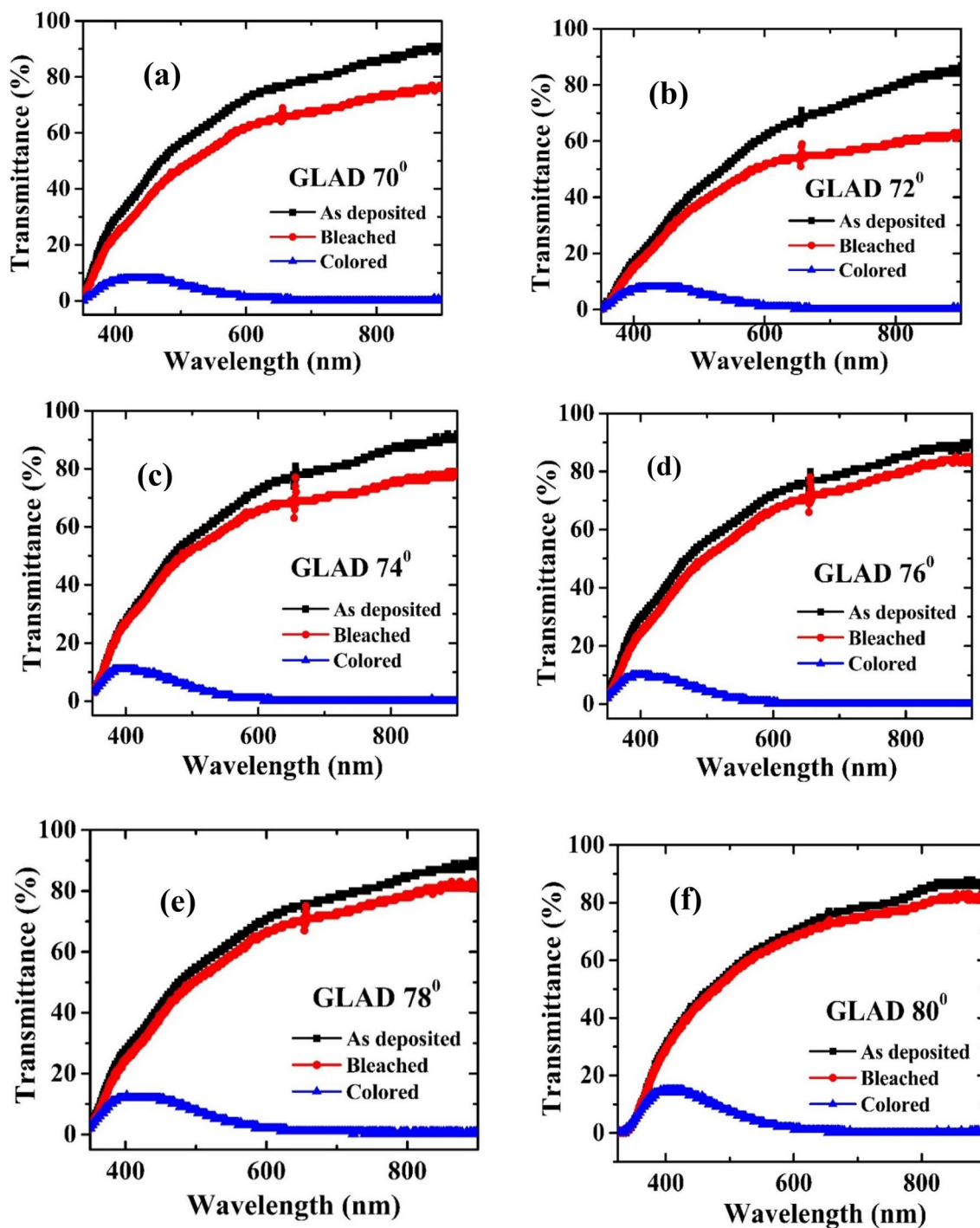


Fig. 4 Transmittance spectra of bleached, as deposited, and colored states of WO_3 films deposited at RT **a** 70° , **b** 72° , **c** 74° , **d** 76° , **e** 78° , **f** 80°

angles. In RT samples GLAD angle 76° shows a high CE from $54.5 \text{ cm}^2/\text{C}$ (at $\lambda = 600 \text{ nm}$) compare to all GLAD angles and in annealed samples GLAD angle

76° shows a high CE from $28.8 \text{ cm}^2/\text{C}$ (at $\lambda = 600 \text{ nm}$) compare all GLAD angles. Diffusion coefficient vs GLAD angles are shown in Fig. 7 and charge vs time

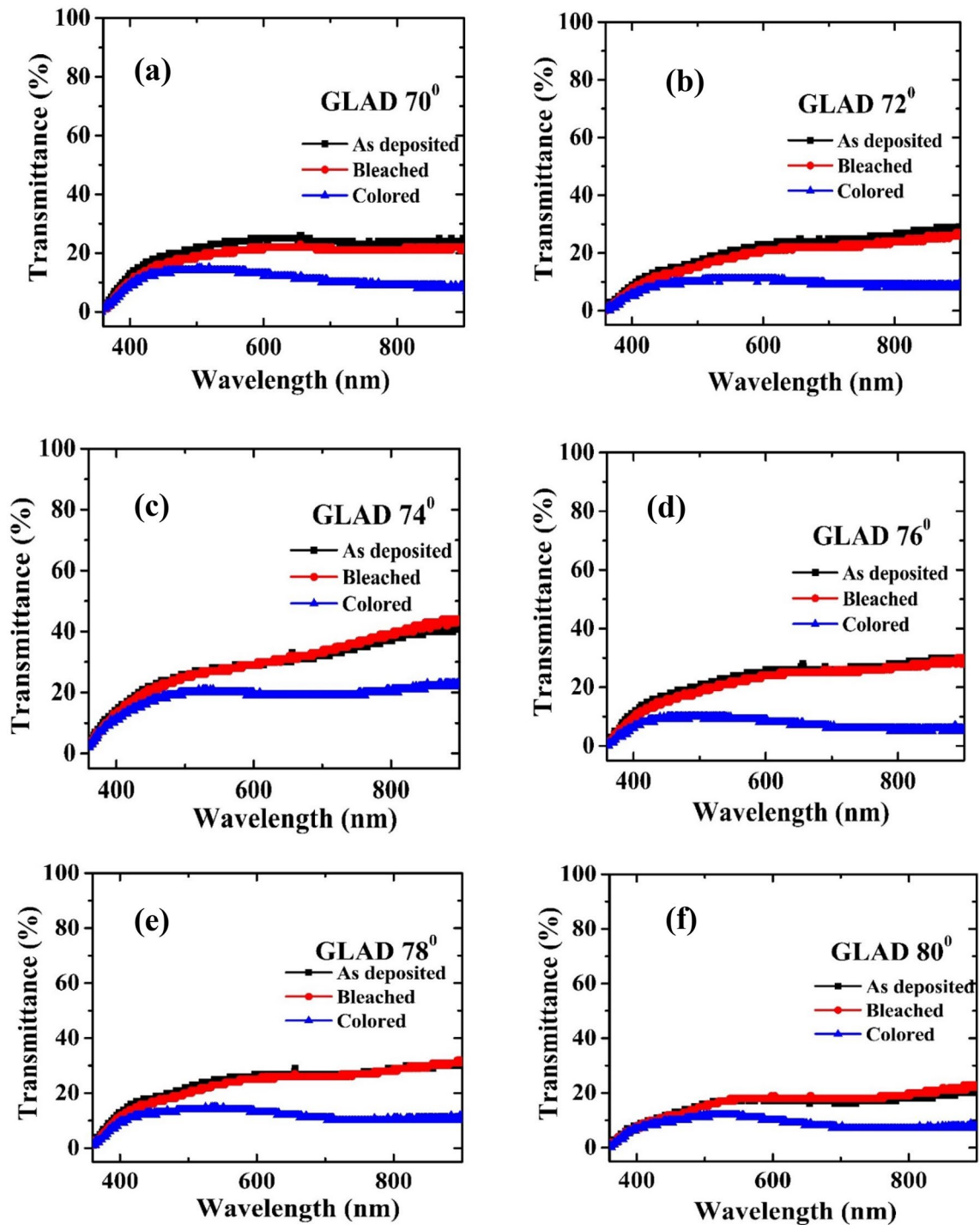


Fig. 5 Transmittance spectra of bleached, as deposited, and colored states of WO_3 films annealed at 400 °C **a** 70°, **b** 72°, **c** 74°, **d** 76°, **e** 78°, and **f** 80°

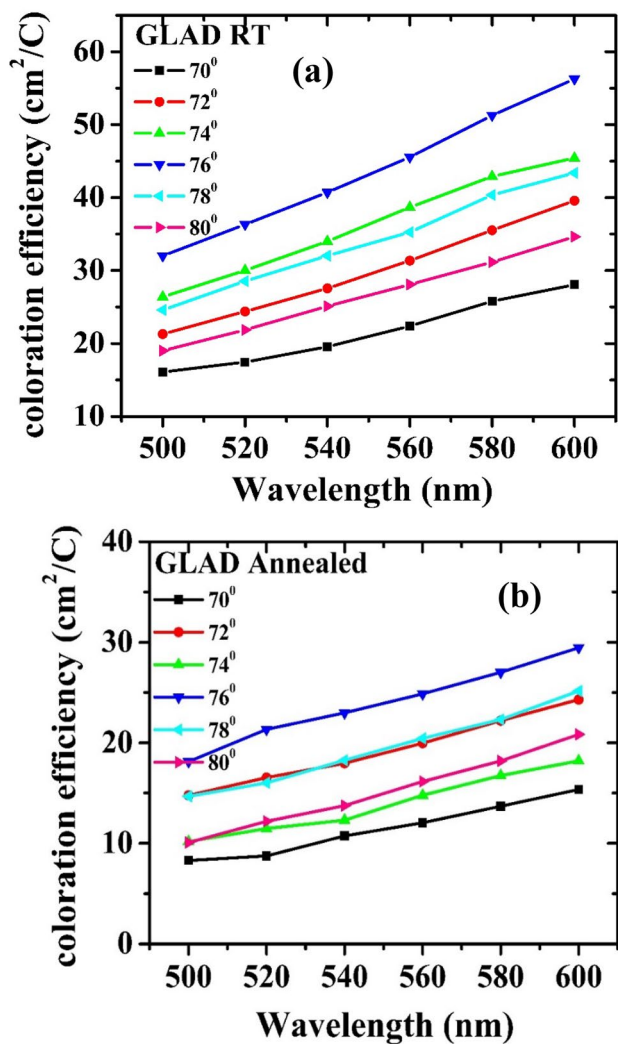


Fig. 6 CE of WO₃ samples for all GLAD angles a RT and b Annealed

is shown in Fig. 8. Diffusion coefficient means how many H⁺ ions are intercalated and de-intercalated in the EC layer and how the charge was varying in the intercalation and de-intercalation process. The calculated diffusion coefficient of nanocolumnar structured WO₃ thin film for RT and annealed samples is shown in Table 1. Obviously, the film with a nanocolumnar structure has a greater Hydrogen ion diffusion coefficient, which may be attributed to the large specific

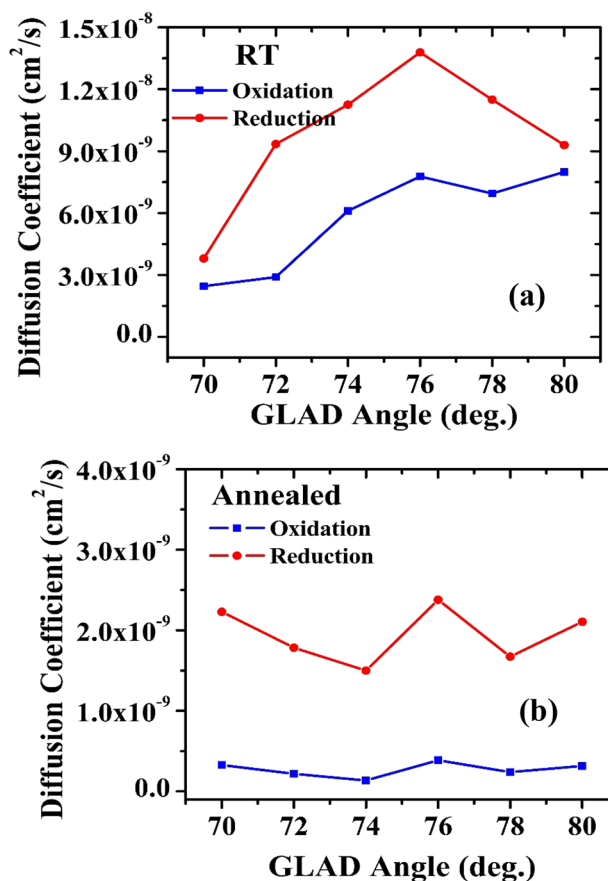


Fig. 7 Diffusion coefficient of WO₃ samples for all GLAD angles a RT and b annealed

surface area and shorter pathway. RT samples show the nanocolumnar structured WO₃ thin film with a larger Hydrogen ion diffusion coefficient has higher capacity when colored/bleached at higher rates and possesses fast response performance compared to the annealed samples.

3.4 Surface analysis

The SEM images of WO₃ films were deposited on CG substrates by using the GDMS at a substrate angle of 76° as shown in Fig. 9. Figure 9a, b show the surface and cross-sectional images of WO₃ films deposited

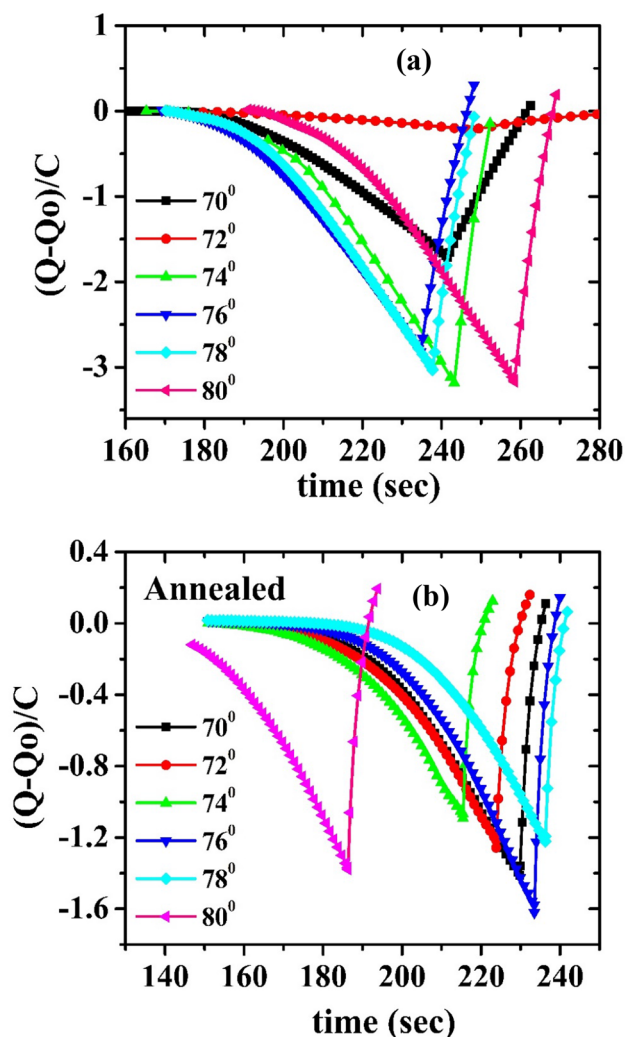


Fig. 8 Charge vs time of WO_3 samples for all GLAD angles **a** as-deposited **b** Annealed

at a substrate angle of 76° at RT and thickness were maintained at 500 nm. The RT-deposited samples were shown porous structure compared to Fig. 9c, d annealed samples. The RT WO_3 film's distinct microstructure efficiently increases the electrode/electrolyte contact areas and facilitates the transfer of electrons and ions during the EC process. Along with the temperature increasing, the surface morphologies of the films change significantly. Compared to the as-deposited sample, the columns are more closely packed, and the porosity of the sample reduces at the annealing temperature of 400°C [34]. From the Figs. 9a and b, Fig. 9a shows the more porous structure due to this most of the electrolyte reacts with the WO_3 material and Fig. 9c shows after the annealing the columns are more closely packed, and the porosity of the sample reduces to this less electrolyte is reacted to the WO_3 material.

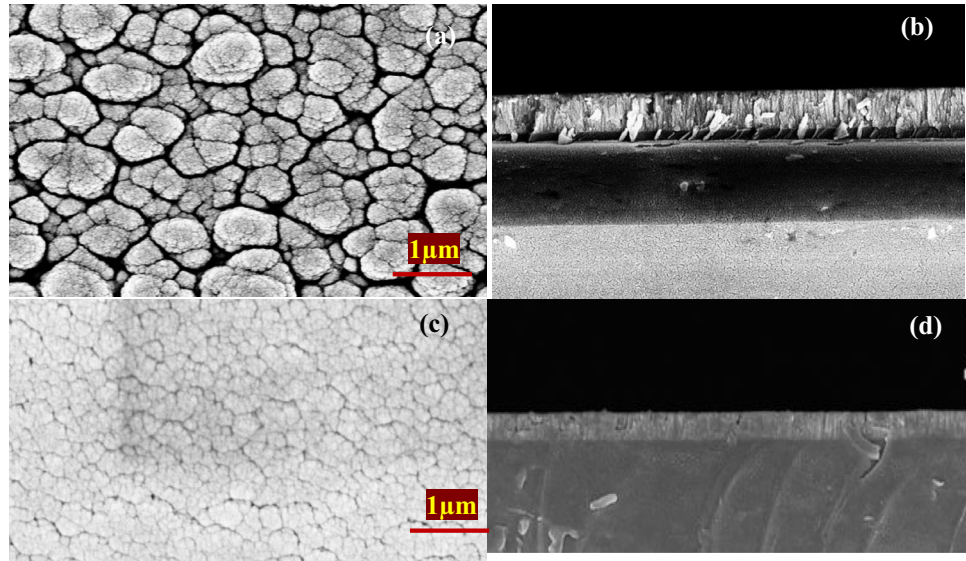
4 Conclusions

WO_3 films were obtained from the GLAD DC magnetron sputtering deposition method and substrate angles were varied from 70° to 80° . The tungsten oxide (WO_3) thin films were deposited on FTO and CG substrates. WO_3 films were deposited at RT and annealed at $400^\circ\text{C}/2\text{ h}$. The structural, optical, and electrochromic properties have been studied systematically. According to the XRD data, RT-deposited samples exhibit an amorphous nature, while annealed samples exhibit a crystalline structure. Compared to the RT samples annealed samples transmittance is decreased. The coloration

Table 1 Ions Intercalation and de-intercalation diffusion rates of WO_3 films for RT and annealed samples

Glad angles	Ion diffusion coefficient ($\text{cm}^2\text{ s}^{-1}$) of RT samples		Ion diffusion coefficient ($\text{cm}^2\text{ s}^{-1}$) of annealed samples	
	Intercalation	De-intercalation	Intercalation	De-intercalation
70°	$2.898\text{E}-9$	$9.346\text{E}-9$	$3.284\text{E}-10$	$2.2292\text{E}-9$
72°	$6.106\text{E}-9$	$1.125\text{E}-8$	$2.189\text{E}-10$	$1.783\text{E}-9$
74°	$7.775\text{E}-9$	$1.379\text{E}-8$	$1.354\text{E}-10$	$1.512\text{E}-9$
76°	$6.950\text{E}-9$	$1.150\text{E}-8$	$3.862\text{E}-10$	$2.378\text{E}-9$
78°	$7.997\text{E}-9$	$9.299\text{E}-9$	$2.390\text{E}-10$	$1.6728\text{E}-9$
80°	$2.898\text{E}-9$	$9.346\text{E}-9$	$3.176\text{E}-10$	$2.105\text{E}-9$

Fig. 9 Crosssectional and surface SEM images of WO_3 films deposited at substrate angles of 76° **a** and **b** RT and **c** and **d** Annealed WO_3 films



efficiency and diffusion coefficient were higher for both RT and annealed films deposited at $G=76^\circ$.

Acknowledgements

The author thanks the Nitte Meenakshi Institute of Technology, Bengaluru, India for providing facilities and the work was supported by the Researchers Supporting Project Number (RSPD2023R765), King Saud University, Riyadh, Saudi Arabia.

Author contributions

KNK, SAS, GVAR, RIJ: investigation, methodology, validation. RP, MRM, AAA, MM, MD, AMT: methodology, validation.

Data availability

All data generated or analyzed during this study are included in this article and are available with the author.

Declarations

Conflict of interest There is no conflict of interest to declare.

References

1. J. Gupta, H. Shaik, K.N. Kumar, A review on the prominence of porosity in tungsten oxide thin films for electrochromism. *Ionics (Kiel)* **27**(6), 2307–2334 (2021). <https://doi.org/10.1007/s11581-021-04035-8>
2. J. Gupta, H. Shaik, K.N. Kumar, S.A. Sattar, PVD techniques proffering avenues for fabrication of porous tungsten oxide (WO_3) thin films: a review. *Mater. Sci. Semicond. Process.* **143**, 106534 (2022). <https://doi.org/10.1016/j.mssp.2022.106534>
3. K.N. Kumar et al., Effect of partial pressure of oxygen, target current, and annealing on DC sputtered tungsten oxide (WO_3) thin films for electrochromic applications. *Solid State Ionics* **399**, 116275 (2023). <https://doi.org/10.1016/j.ssi.2023.116275>
4. H. Simchi, B.E. McCandless, T. Meng, W.N. Shafarman, Structural, optical, and surface properties of WO_3 thin films for solar cells. *J. Alloys Compd.* **617**(302), 609–615 (2014). <https://doi.org/10.1016/j.jallcom.2014.08.047>
5. D. Shao, M. Yu, J. Lian, S. Sawyer, An ultraviolet photo-detector fabricated from WO_3 nanodiscs/reduced graphene

- oxide composite material. *Nanotechnology* (2013). <https://doi.org/10.1088/0957-4484/24/29/295701>
6. J.L. Solis, S. Saukko, L. Kish, C.G. Granqvist, V. Lantto, Semiconductor gas sensors based on nanostructured tungsten oxide. *Thin Solid Films* **391**(2), 255–260 (2001). [https://doi.org/10.1016/S0040-6090\(01\)00991-9](https://doi.org/10.1016/S0040-6090(01)00991-9)
 7. J. Ollitrault, N. Martin, J.Y. Rauch, J.B. Sanchez, F. Berger, Improvement of ozone detection with GLAD WO₃ films. *Mater. Lett.* **155**, 1–3 (2015). <https://doi.org/10.1016/j.matlet.2015.04.099>
 8. K.N. Kumar et al., On ion transport during the electrochemical reaction on plane and GLAD deposited WO₃ thin films. *Mater. Today Proc.* **59**, 275–282 (2022). <https://doi.org/10.1016/j.matpr.2021.11.113>
 9. K.N. Kumar et al., Effect of annealing and oxygen partial pressure on the RF sputtered WO₃ thin films for electrochromic applications. *Mater. Today Proc.* **59**, 339–344 (2022). <https://doi.org/10.1016/j.matpr.2021.11.185>
 10. G.V.A. Reddy et al., Thickness dependent tungsten trioxide thin films deposited using DC magnetron sputtering for electrochromic applications. *Mater. Today Proc.* (2022). <https://doi.org/10.1016/j.matpr.2022.11.134>
 11. T. Sanjana, M.A. Sunil, H. Shaik, K.N. Kumar, Studies on DC sputtered cuprous oxide thin films for solar cell absorber layers. *Mater. Chem. Phys.* **281**, 125922 (2022). <https://doi.org/10.1016/j.matchemphys.2022.125922>
 12. K.N. Kumar et al., Glancing angle sputter deposited tungsten trioxide (WO₃) thin films for electrochromic applications. *Appl. Phys. A* **128**(11), 1–8 (2022). <https://doi.org/10.1007/s00339-022-06124-5>
 13. G.V.A. Reddy et al., Structural and electrochemical studies of WO₃ coated TiO₂ nanorod hybrid thin films for electrochromic applications. *Optik (Stuttg)* **277**, 170694 (2023). <https://doi.org/10.1016/j.ijleo.2023.170694>
 14. K.N. Kumar, G. Nithya, H. Shaik, L.N. Chandrashekar, P. Aishwarya, A.S. Pawar, Optical and electrochromic properties of DC magnetron sputter deposited tungsten oxide thin films at different electrolyte concentrations and vertex potentials for smart window applications. *J. Mater. Sci.* (2023). <https://doi.org/10.1007/s10854-023-10180-9>
 15. G.V.A. Reddy et al., Physica B: condensed matter effect of post annealing on DC magnetron sputtered tungsten oxide (WO₃) thin films for smartwindow applications. *Physica B* **664**, 414996 (2023). <https://doi.org/10.1016/j.physb.2023.414996>
 16. G.V.A. Reddy, S.A. Sattar, C. Devaraja, H.S. Yogananda, Effect of growth fluid concentration on characteristics of CeO₂ nanorods and WO₃/CeO₂ nanostructured hybrid films for electrochromic applications. *J. Mater. Sci.* (2023). <https://doi.org/10.1007/s10854-023-10850-8>
 17. G.V.A. Reddy, K.N. Kumar, H.D. Shetty, C. Devaraja, M. Dhananjaya, S.M. Hunagund, Materials today: proceedings comparison study of WO₃ thin film and nanorods for smart window applications. *Mater. Today Proc.* (2023). <https://doi.org/10.1016/j.matpr.2023.03.052>
 18. J. Gupta, H. Shaik, K.N. Kumar, S.A. Sattar, G.V.A. Reddy, Optimization of deposition rate for E-beam fabricated tungsten oxide thin films towards profound electrochromic applications. *Appl. Phys. A* **128**(6), 1–15 (2022). <https://doi.org/10.1007/s00339-022-05609-7>
 19. J. Gutpa, H. Shaik, K.N. Kumar, S.A. Sattar, Optimization of GLAD angle for E-beam-fabricated tungsten oxide (WO₃) thin films towards novel electrochromic behavior. *J. Electron. Mater.* (2022). <https://doi.org/10.1007/s11664-022-10036-8>
 20. K.J. Patel et al., Thickness-dependent electrochromic properties of Amorphous tungsten trioxide thin films. *J. Nano-Electron. Phys.* (2017). [https://doi.org/10.21272/jnep.9\(3\).03040](https://doi.org/10.21272/jnep.9(3).03040)
 21. K. Robbie, M.J. Brett, Sculptured thin films and glancing angle deposition: growth mechanics and applications. *J. Vac. Sci. Technol. A* **15**(3), 1460–1465 (1997). <https://doi.org/10.1116/1.580562>
 22. V.V. Kondalkar et al., Nanobrick-like WO₃ thin films: hydrothermal synthesis and electrochromic application. *Superlattices Microstruct.* **73**, 290–295 (2014). <https://doi.org/10.1016/j.spmi.2014.05.039>
 23. G.V.A. Reddy, K.N. Kumar, R. Naik, V. Revathi, K.M. Girish, K. Munirathnam, Applied surface science advances comparative analysis of the effect of post-annealing on CeO₂ and DC magnetron sputtered WO₃/CeO₂ nanorods thin films for smart windows. *Appl. Surf. Sci. Adv.* **16**, 100417 (2023). <https://doi.org/10.1016/j.apsadv.2023.100417>
 24. G.V.A. Reddy et al., Growth of cerium oxide nanorods by hydrothermal method and electrochromic properties of CeO₂/WO₃ hybrid thin films for smart window applications. *Mater. Today Proc.* (2022). <https://doi.org/10.1016/j.matpr.2022.11.316>
 25. G.V.A. Reddy et al., Effect of tungsten oxide thin films deposited on cerium oxide nano rods for electrochromic applications. *Opt. Mater. (Amst.)* **134**, 113220 (2022). <https://doi.org/10.1016/j.optmat.2022.113220>
 26. G.V.A. Reddy et al., Structural, optical, and electrochromic properties of rare earth material (CeO₂)/transitional metal oxide (WO₃) thin film composite structure for electrochromic applications. *Ionics (Kiel)* (2023). <https://doi.org/10.1007/s11581-023-05078-9>
 27. G.V.A. Reddy et al., Synthesis, characterizations, and electrochromic studies of WO₃ coated CeO₂ nanorod thin films

- for smart window applications. *Physica B* **647**, 414395 (2022). <https://doi.org/10.1016/j.physb.2022.414395>
28. K. Robbie, Advanced techniques for glancing angle deposition. *J. Vac. Sci. Technol. B* **16**(3), 1115 (1998). <https://doi.org/10.1116/1.590019>
29. C. Charles, N. Martin, M. Devel, J. Ollitrault, A. Billard, Correlation between structural and optical properties of WO₃ thin films sputter deposited by glancing angle deposition. *Thin Solid Films* **534**, 275–281 (2013). <https://doi.org/10.1016/j.tsf.2013.03.004>
30. V. Madhavi et al., Fabrication of porous 1D WO₃ NRs and WO₃/BiVO₄ hetero junction photoanode for efficient photoelectrochemical water splitting. *Mater. Chem. Phys.* **274**, 125095 (2021). <https://doi.org/10.1016/j.matchemphys.2021.125095>
31. M. Horprathum et al., NO₂-sensing properties of WO₃ nanorods prepared by glancing angle DC magnetron sputtering. *Sens. Actuators B* **176**(2), 685–691 (2013). <https://doi.org/10.1016/j.snb.2012.09.077>
32. M. Layani et al., Nanostructured electrochromic films by inkjet printing on large area and flexible transparent silver electrodes. *Nanoscale* **6**(9), 4572–4576 (2014). <https://doi.org/10.1039/c3nr06890k>
33. J. Yuan et al., Electrochromic behavior of WO₃ thin films prepared by GLAD. *Appl. Surf. Sci.* **447**, 471–478 (2018). <https://doi.org/10.1016/j.apsusc.2018.03.248>
34. A. Rydosz, K. Dyndał, K. Kollbek, W. Andrysiewicz, M. Sitarz, K. Marszałek, Structure and optical properties of the WO₃ thin films deposited by the GLAD magnetron sputtering technique. *Vacuum* (2020). <https://doi.org/10.1016/j.vacuum.2020.109378>
35. J.J. Steele, M.J. Brett, Nanostructure engineering in porous columnar thin films: recent advances. *J. Mater. Sci.* **18**(4), 367–379 (2007). <https://doi.org/10.1007/s10854-006-9049-8>
36. A. Hrubantova et al., Deposition of tungsten oxide films by reactive magnetron sputtering on different substrates. *J. Vac. Sci. Technol. A* **40**(6), 063402 (2022). <https://doi.org/10.1116/6.0002012>

Publisher's Note Springer Nature remains neutral with regard to jurisdictional claims in published maps and institutional affiliations.

Springer Nature or its licensor (e.g. a society or other partner) holds exclusive rights to this article under a publishing agreement with the author(s) or other rightsholder(s); author self-archiving of the accepted manuscript version of this article is solely governed by the terms of such publishing agreement and applicable law.